JOURNAL OF AIRCRAFT
Vol. 39, No. 6, November–December 2002

Unsteady Aerodynamic Analysis of Tandem Flat Plates in Ground Effect

Cheolheui Han*
Hanyang University, Seoul 133-791, Republic of Korea
Younghyun Yoon†
Korea Air Force Academy, Chungwon 363-849, Republic of Korea
and
Jinsoo Cho‡
Hanyang University, Seoul 133-791, Republic of Korea

Unsteady aerodynamic analysis of flat plates in tandem configuration flying near the ground is done using a discrete vortex method. The vortex core modeling and the core addition scheme are needed for the better prediction of the unsteady downwash on the flat plates and coupled aerodynamic interference between the plates. For the validation of the present method, the computed wake shapes of both single flat plate and flat plates in tandem configuration are compared with flow visualization and other numerical results. The predicted wake shapes and the aerodynamic characteristics of the flat plates in tandem configuration show that the unsteady ground effect can be of considerable importance in the performance of wings in tandem configuration.

Nomenclature

A_{ij}	=	normal component of velocity induced at control point i by a unit circulation at node j
c	=	chord length
$H_{0.25C}$	=	distance between quarter-chord point and the ground
$H_{0.5C}$	=	distance between half-chord point and the ground
$h_{0.25}$	=	$H_{0.25C}/c$
$h_{0.5}$	=	$H_{0.5C}/c$
h_0	=	heaving oscillation amplitude
l	=	distance between the quarter-chord points of plates
N	=	number of nodes on a flat plate
NT	=	number of total time steps
$\boldsymbol{n}_i$	=	unit normal vector at control point i
p_0	=	pitching oscillation amplitude
Q_i	=	normal velocity induced at control point i by a unit circulation at the trailing edge
R_c	=	cylinder Reynolds number
r_c	=	vortex core radius
t, T	=	time
U_∞	=	freestream velocity
X, Y	=	ground-fixed coordinates
x, y	=	body-fixed coordinates
α	=	angle of attack
Γ	=	circulation of a point vortex
γ	=	flight-path angle
Δl	=	panel length
$\Delta t, \Delta T$	=	time step
θ	=	pitch angle
ρ	=	freestream density
Φ	=	velocity potential
ω	=	heaving oscillation frequency
ω_p	=	pitching oscillation frequency

Received 13 April 2001; presented as Paper 2001-2471 at the AIAA 19th Applied Aerodynamics, Anaheim, CA, 11–14 June 2001; revision received 11 July 2002; accepted for publication 20 July 2002.

*Graduate Student, School of Mechanical Engineering. Member AIAA.
†Professor, Department of Aerospace Engineering. Member AIAA.
‡Professor, School of Mechanical Engineering. Senior Member AIAA.

I. Introduction

THE over-the-ground-surface type wing-in-ground (WIG) effect vehicles such as the high-speed guide way train (Aero-Train)[1] are free from the surface conditions caused by the ground rigidity. They can fly faster at a very low altitude compared to the over-the-water-surface type WIG vehicles. According to the studies[1,2] in relation to the steady (static) ground effect on wings in tandem configuration, it has been known that they have a good pitching stability near the ground. Thus, several over-the-ground-surface type WIG vehicles are proposed to have wings in tandem configuration. However, the unsteady (dynamic) ground effect can give rise to the significant change on the aerodynamic characteristics of wings. To develop such vehicles, the basic research on the ground effect is crucial for the reliable prediction of the WIG vehicle performances.

Chen and Schweikhard[3] addressed the dynamic ground effect by considering a flat plate descending to the ground from a high altitude. Their results have the limitation by using the fixed wake path. Nuhait and Zedan[4] studied the dynamic ground effect by allowing wakes to deform and roll up freely according to its force-free position. Katz[5] used a vortex-lattice method that also included a freely deforming wake to investigate the ground effect on the lift of wings used for a racing car. Nuhait and Mook[6] developed a general model of finite lifting surfaces in steady and unsteady ground effect. Recently, Rozhdestvensky[7] gave an extensive review for analytical, computational, and experimental researches on the WIG effect. However, not much is shown in the literature in relation to the dynamic ground effect on wings in tandem configuration.

In this paper the dynamic ground effect on the aerodynamic characteristics of flat plates in tandem configuration is investigated by using a discrete vortex method. To analyze the closely coupled aerodynamic interference between the flat plates, an accurate simulation of the near-field and medium-field wake is required. The improperly simulated wake shapes can cause the inaccurate predictions of aerodynamic coefficients. Sarpaka[8] addressed the numerical instabilities arising from a discrete vortex method. Mook et al.[9] solved the problem by introducing a vortex core addition scheme. In this paper the core addition scheme[9] and a vortex core model[10] are combined together. A calculated wake pattern for a flat plate in heaving oscillation motion is compared with the flow visualization. The effect

of the vortex core modeling[10] and the core addition scheme[9] can be validated by comparing the results with the time-step reduction scheme. The present method is also validated for a front airfoil pitching around the quarter-chord axis and a rear stationary airfoil in its wake.[9] The wake shapes and the aerodynamic characteristics of flat plates in tandem configuration are predicted.

II. Method of Analysis

To treat the unsteady motions of flat plates moving through the air, two coordinate systems are used (Fig. 1): the body-fixed coordinate system (x, y) and the inertial frame of reference (X, Y). The flow is assumed to be inviscid, incompressible, and irrotational over the entire flowfield, excluding the flat plates' solid boundaries and their wakes. A velocity potential $\Phi(X, Y)$ can be defined in the inertial frame, and the continuity equation becomes the Laplace equation. Mass should be conserved regardless of the coordinate systems. Therefore, the continuity equation in terms of (x, y) remains unchanged.

$$\nabla^2\Phi = 0 \quad (\text{in } x, y \text{ coordinates}) \tag{1}$$

The solution of Eq. (1) can be obtained by the distribution of elementary solutions. A flat plate is discretized into $(N-1)$ equal length panel elements. The vorticity on each element is considered as uniform. The vorticity of uniform strength on each element is replaced by a point vortex of strength Γ_j located at a distance equal to $\frac{1}{4}$ of the element length behind its leading edge, as shown in Fig. 2. The wake is represented by free vortices that deform freely by the assumption of a force-free position during the simulation. These free vortices are connected to the bound vortices at the trailing edge of the plate through the Kutta condition. The strengths of the elementary solutions are obtained by enforcing some boundary conditions as follows:

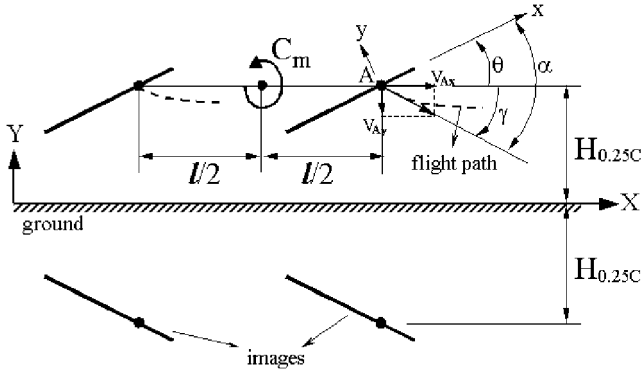

Fig. 1 Coordinate systems: γ (flight-path angle), θ (pitch angle), α (angle of attack), c (chord length), V_{Ax}, V_{Ay} (X, Y component of the plate velocity), $H_{0.25C}$ (height of the quarter-chord point above the ground), $h_{0.25}(H_{0.25C}/c)$, l (distance between quarter-chord points of the plates), C_m (total moment coefficient of the plates in tandem configuration).

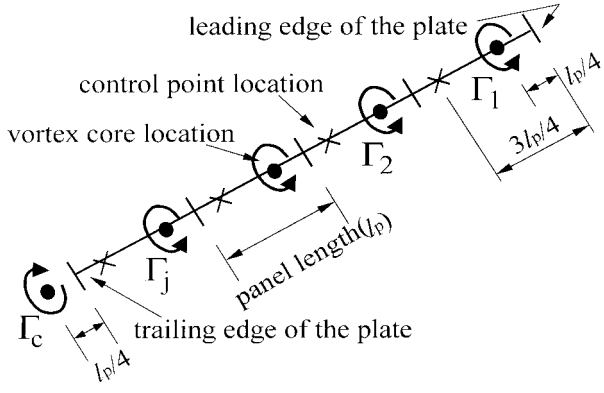

Fig. 2 Discretization of a flat plate.

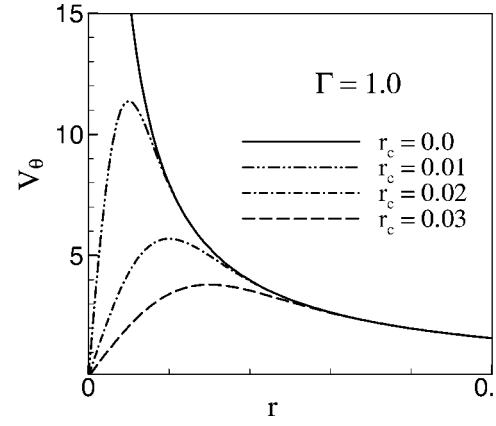

Fig. 3 Circumferential velocities for various core radii.

1) The flow disturbance, caused by the plates' motion through the fluid, should vanish far from the plates. This boundary condition can be satisfied automatically by using the discrete vortices as the singularity distributions.

2) Zero normal flow across the plates' solid boundaries is the next boundary condition. The continuity equation (1) does not directly include time-dependent terms. Time dependency is introduced through the modification of "zero normal flow on a solid surface" and the use of the unsteady Bernoulli equation. If the kinematic velocity $(\boldsymbol{v})$ is given as follows,

$$\boldsymbol{v} = -(\boldsymbol{V}_0 + \boldsymbol{v}_{\text{rel}} + \boldsymbol{\Omega} \times \boldsymbol{r}) \tag{2}$$

where $\boldsymbol{v}_0$ is the velocity of the body-fixed system's origin, $\boldsymbol{r} = (x, y, z)$ is the position vector, $\boldsymbol{\Omega}$ is the rate of rotation of the body's frame of reference, and $\boldsymbol{v}_{\text{rel}}$ is the additional relative motion within the (x, y, z) system.

The zero-velocity normal to a solid surface boundary in the body-fixed frame becomes

$$(\nabla\Phi - \boldsymbol{V}_0 - \boldsymbol{v}_{\text{rel}} - \boldsymbol{\Omega} \times \boldsymbol{r}) \cdot \boldsymbol{n} = 0 \qquad (\text{in } x, y \text{ coordinates}) \tag{3}$$

where $\boldsymbol{n}$ is the normal to the body's surface, in terms of the body coordinates (x, y). The plate is considered rigid; hence, $\boldsymbol{v}_{\text{rel}}$ is equal to zero. Also, $\boldsymbol{\Omega}$ is assumed to be zero. Fulfilling the boundary condition on the surface requires that, at each collocation point, the normal velocity component will vanish, and we can write Eq. (3) as

$$\sum_{j=1}^{N-1} a_{ij}\Gamma_j - q_i\Gamma_c = (\boldsymbol{V}_0 - \boldsymbol{V}_{\text{wi}}) \cdot \boldsymbol{n}_i \qquad \text{on the plate for} \quad i = 1, 2, \ldots, N-1 \tag{4}$$

where the influence matrix element a_{ij} represents the normal velocity component at a control point i by the point vortex (having a unit circulation) at the panel element j and its image; elements a_{ij} are functions of geometry; Γ_j is the unknown circulation of the point vortex representing the vorticity of the panel element j; q_i represents the normal velocity component induced at control point i by the starting vortex and its image; and $\boldsymbol{V}_{\text{wi}}$ is the velocity induced by the wake vortices and their images whose positions and circulations are known. At the beginning $\boldsymbol{V}_{\text{wi}}$ is zero. The calculation begins at $t = \Delta t$, and the wake at this moment consists of a single vortex Γ_c. Following Mook et al.,[9] we simulate this starting vortex by placing it at a point of $\frac{1}{4}$ behind an airfoil trailing edge (Fig. 2).

3) The third boundary condition is the Kelvin condition. The use of Kelvin condition, which shows the circulation around a fluid curve enclosing the plates and how their wakes are conserved, will supply an additional equation

$$\sum_{j=1}^{N-1} \Gamma_j - \Gamma_c = \sum_{j=1}^{NT-1} \Gamma_{\text{wake}} \tag{5}$$

Γ_{wake} is the circulation of a wake core at node k, which is zero at the start of motion. The wake is created as a result of shedding and convecting the starting vortex at each time step.

4) The unsteady Kutta condition at the trailing edge of a plate is satisfied by shedding the vorticity generated at the trailing of a plate at the local fluid particle velocity.

5) The condition of continuous pressure across the wake is fulfilled with convecting wakes downstream at the local fluid particle velocity.

To solve Eqs. (4) and (5), an initial condition describing the position of the wake and its vorticity must be prescribed. At each time step a newly shed starting vortex is fixed at a point of $\frac{1}{4}$ behind a plate's trailing edge, as required by the unsteady Kutta condition. All of the circulation strengths are determined including the effects of their images by the Gauss elimination. At the end of the step, the shed vortex is convected downstream to its new position at the local fluid particle velocity. The procedure is repeated for any desired number of time steps.

A. Wake Roll up

Because the wake is force free, each vortex representing the wake must move with the local flow velocity. The local flow velocity is the result of the velocity components induced by the wake and the plate. It is measured in the inertial frame of reference (X, Y). To achieve the vortex wake roll up at each time, the induced velocity $(u, v)_i$ at each vortex wake point i is calculated, and then the vortex elements are moved by Euler convection scheme.

$$(\Delta x, \Delta y)_i = (u, v)_i \Delta t \tag{6}$$

The induced velocity is calculated by using the Biot–Savart law. Sarpaka[8] addressed the two difficulties with the Biot–Savart approach for two-dimensional simulations using line vortices. 1) The vortex filament singularities cause numerical instabilities and physically impossible sheet crossings along the wake vortex sheet. 2) Because the computing time is proportional to m^2, where m is the number of vortices,[8] the significant increase in CPU time occurs as more vortices are added. They also reviewed numerous schemes and hybrid methods to overcome the preceding difficulties. In 1986 Mook et al.[9] contrived a core addition scheme alternative to a redistribution scheme described by Sarpkaya and Schoaff.[11] Their scheme was effective in simulating unsteady aerodynamic interferences. However, another method is necessary to decrease computing time. In this paper the computing time is minimized by combining a core addition scheme[9] and the vortex core modeling,[10] which will be shown later.

B. Vortex Core Addition Scheme

In the regions where vortex cores are separating, leaving big gaps and beginning to reassemble, the unequal spacing between the cores could lead to serious computational problems. The core addition scheme[9] imitates the elongated region of the vorticity in the actual flow.[12] If the distance between two successively shedding cores is separated by more than a prescribed "critical length," a new core is located at the midpoint of the line segment connecting them. This new core has $\frac{1}{3}$ the sum of circulations around the two original cores. The circulations around the two original cores are reduced by a factor of $\frac{2}{3}$.

C. Vortex Core Model

A real vortex is not a concentrated singularity of infinite vorticity. The best known models for a real vortex are the Rankine and the Lamb (Oseen) model.[13] The Rankine vortex rotates as a solid body within a core. The Lamb model involves the Gaussian vorticity distribution. Ling et al.[10] employed a more advanced technique based upon the solution for the actual velocity induced by a vortex in a viscous fluid. A core radius r_c at time t is approximately equal to the radial distance of the point where the maximum velocity is induced.

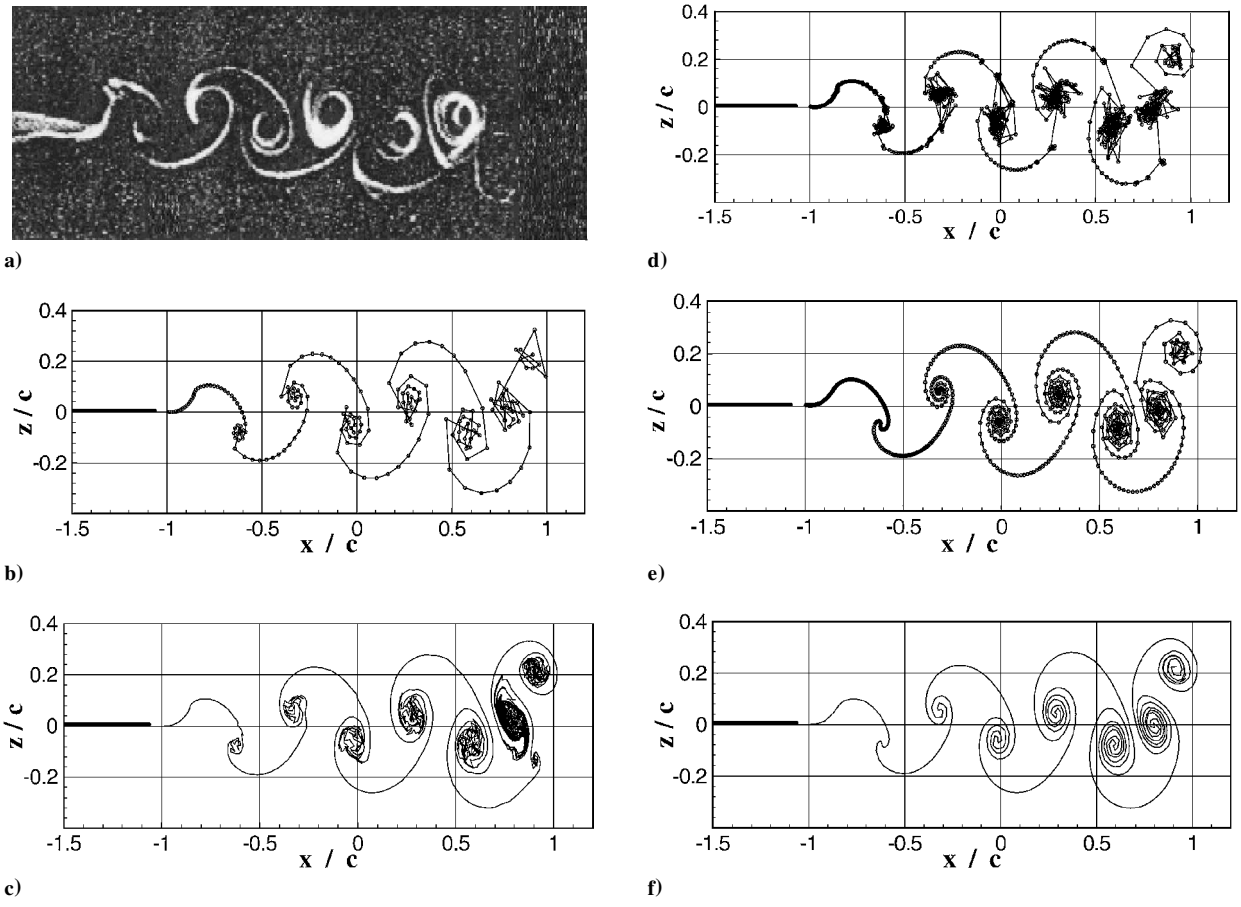

Fig. 4 Wake patterns behind a flat plate undergoing heaving oscillation motion.

This can be expressed for an element j in terms of its initial core radius r_{cj0} and growth age Δt_j through

$$r_{\mathrm{cj}} = r_{\mathrm{cj0}} + 3.17\sqrt{\Delta t_j / R_c} \tag{7}$$

where $R_c = U_\infty D/\nu$ is the cylinder Reynolds number. The velocity within the core (v_j) is

$$v_j = (\Gamma_j/2\pi r)\left\{1 - \exp\left[-1.25643(r/r_{\mathrm{cj}})^2\right]\right\} \tag{8}$$

where Γ_j is a strength of a vortex and r is the distance between the origin of the vortex core and the point in space. Outside the core region the induced velocity can be taken as that of a free vortex of strength Γ_j (Fig. 3).

D. Image Method

Following Wieselsberger,[14] the ground effect is included by the image method. The ground is simulated by placing the image of a flat plate at an equal distance below the ground as shown in Fig. 1. Two symmetrically positioned lifting surfaces are considered to create a straight streamline along the ground plane.

E. Extension to Flat Plates in Tandem Configuration

By fulfilling the zero-normal flow boundary condition on each plate, $2(N-1)$ equations are constructed. The use of the Kelvin condition at each plate adds two more equations. Thus, the constructed aerodynamic influence matrix becomes determinant. The Kutta condition is also satisfied at the trailing edge of each plate.

F. Computation of Aerodynamic Loads

In the body-fixed frame the pressure difference ($p_\infty - p$) can be computed by the unsteady Bernoulli equation

$$\frac{p_\infty - p}{\rho} = \frac{1}{2}\left[\left(\frac{\partial \Phi}{\partial x}\right)^2 + \left(\frac{\partial \Phi}{\partial y}\right)^2\right] + \boldsymbol{v}_{\mathrm{ref}} \cdot \nabla\Phi + \frac{\partial \Phi}{\partial t} \tag{9}$$

where the kinematic velocity $\boldsymbol{v}_{\mathrm{ref}} = -(\boldsymbol{V}_0 + \boldsymbol{\Omega} \times \boldsymbol{r})$.

III. Results and Discussion

Figure 4 shows the wake patterns behind a flat plate undergoing heaving oscillations with $\alpha = 0$, $h_0 = 0.019$, and $\omega c/2U = 8.5$. The required computing time and vortex core numbers are given in Table 1. A desktop computer (Pentium II 333 Mhz CPU and a 160 Mb RAM) is used for the calculation. In Fig. 4a the experimental result of Bratt[15] is shown for an airfoil. Figure 4b shows a computed result without using a scheme. The time step (Δt) is set to 0.01. In the figure the vortex sheet crossing is clearly shown. Figure 4c shows that the use of the core addition scheme[9] with $L_{\mathrm{cr}} = 5.0$ eliminates the unequal spacing between the cores. However, this scheme requires a large amount of computing time without improving the result. Figure 4d shows the poor representation of the wake pattern caused by a time-step reduction scheme ($\Delta t = 0.0027$). It needs the largest computing time among the results as given in Table 1. As shown in Fig. 4e, the computed results are improved using a vortex core model[10] with $r_c = 0.03c$. In Fig. 4f the computing time is minimized by combining a core addition scheme[9] and the vortex core modeling[10] while the computed results show good agreement with the flow visualization.

Figure 5 shows the wake behavior behind a flat plate impulsively started and undergoing a heaving oscillation mode with $\alpha = 0$, $h_0 = 0.019$, $\omega c/2U = 8.5$, and $h_{0.25} = 0.1$. The time step (Δt) is set to $0.009c/U$, the core radius (r_c) $= 0.025c$, and the critical length (L_{cr}) $= 3.0\Delta t U$. At $t = 0.369$ wake vortices are shed from the plate's trailing edge and bounded by the ground. At $t = 0.549$ the wake shape becomes asymmetric. At $t = 0.729$ the wake structure is distorted and becomes complicated. At $t = 0.999$ and 1.296 the wake structures are completely distorted. It can be deduced from the figures that the complicated wake shape at $t = 1.296$ can be predicted well by the present method.

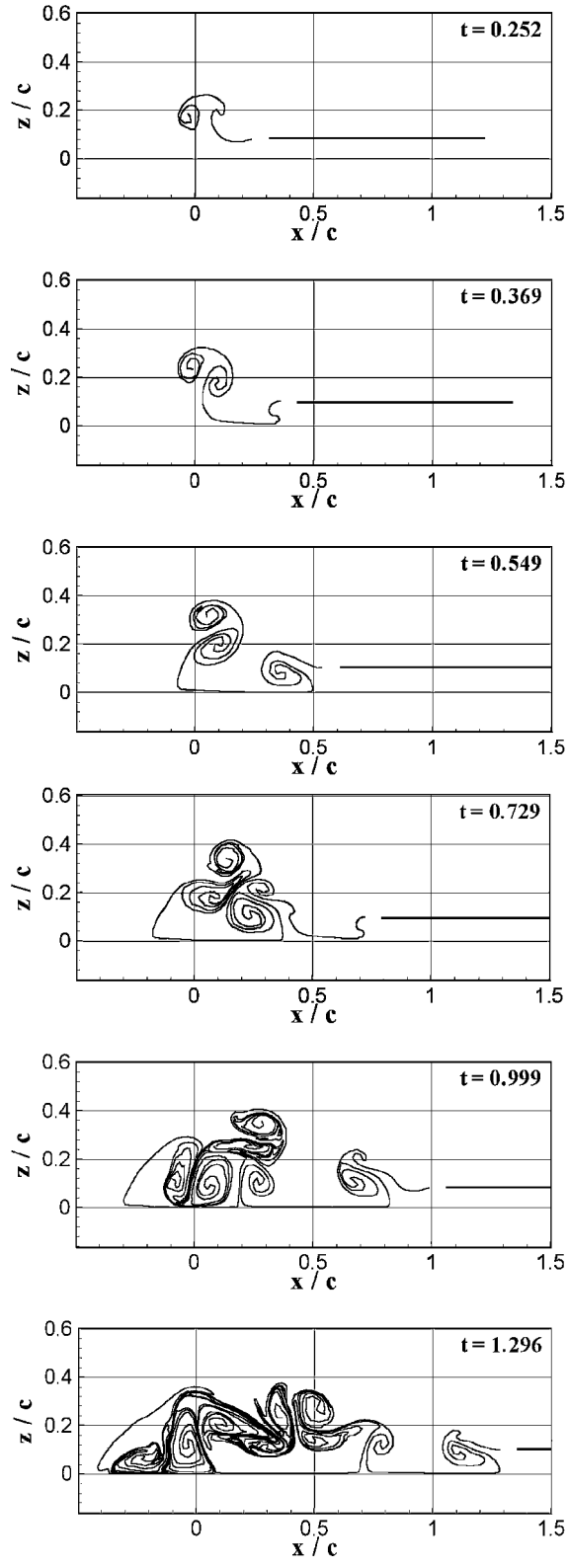

Fig. 5 Wake behavior behind a flat plate in heaving oscillation motion near the ground.

In Fig. 6 the wake pattern calculated by the present method is compared with that of Mook et al.[9] for a front NACA0012 airfoil in simple harmonic pitching oscillation ($p_0 = 0.2$, $\omega_p = 0.8\pi \times 2U_\infty/c$, $U_\infty/c = 1.0$) around the quarter-chord point and a stationary rear NACA0012 airfoil. It can be seen in Figs. 6a and 6b that,

Table 1 Comparison of the required computing time

Case in Fig. 4	Δt $(\times c/U_\infty)$	r_c $(\times c)$	L_{cr} $(\times U_\infty \Delta t)$	Number of cores	Computing time, s
a)	Experimental result	Experimental result	Experimental result	Experimental result	Experimental result
b)	0.01	×	×	200	39.0
c)	0.01	×	5.0	2038	1027.64
d)	0.0027	×	×	740	1705.61
e)	0.0027	0.03	×	740	1678.94
f)	0.01	0.03	5.0	740	263.09

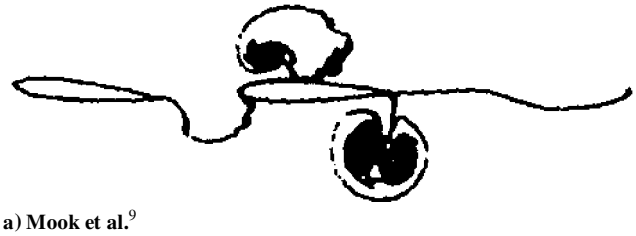

a) Mook et al.[9]

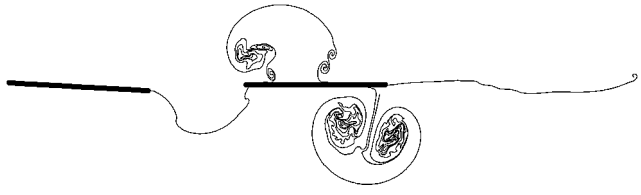

b) Present method

Fig. 6 Wake pattern for a front airfoil pitching around the quarter-chord and a rear stationary airfoil.

although the present result is for the flat plates whereas Mook et al.[9] used the NACA0012 airfoils, the results agree well. In the present calculation $\Delta t = 0.01 \times c/U_\infty$, $r_c = 0.02c$, and $L_{cr} = 1.0\Delta t U_\infty$.

Figure 7 shows the wake shapes and lift coefficients for the flat plates in sudden acceleration motion with $\alpha = 10$ and $l = c$. The out-of-ground effect is shown in Fig. 7a, whereas the in-ground effect for $h_{0.25} = 0.25$ is shown in Fig. 7b. Figure 7 shows that the lift coefficient of the rear plate increases until the wake vortices shed from the front plate drifted toward the rear plate's leading edge. After the vortices pass the rear plate and move further downstream, the lift coefficient of the rear plate decreases. It can be deduced from the figures that the ground effect causes the lift to increase in the rear plate.

Figure 8 shows the wake shapes and lift coefficients for tandem plates in heaving oscillation motion with $\alpha = 0$, $l = 0.7c$, and $\omega c/2U = \pi$. As the wake vortices from a front plate are convecting downstream, they are divided as two parts: some cores pass over the top of a rear plate while others pass along the bottom. Figure 8a shows the lift coefficient oscillation of the rear plate around that of the front plate. Figure 8b shows the higher frequency lift coefficient oscillations for the plates in ground effect with $h_{0.25} = 0.1$ and $h_0 = 0.01$. The complicated aerodynamic interference between the plates and the ground causes severe lift fluctuation in the rear plate.

Figure 9 shows the aerodynamic coefficients of the plates with steady (static) and unsteady (dynamic) ground effect. In the figure the plates are descending to the ground with $\alpha = 12$, $\gamma = 10$, and $l = 2c$. In the figure the total lift coefficients represent the sum of the lift coefficients for both plates. The pitching-moment coefficients are calculated relative to a midpoint between the plates' leading edge. As the plates approach the ground, the total lift coefficients of the plates in dynamic ground effect become bigger than those of the plates in static ground effect. The pitching-moment coefficients for the plates in static ground effect become negative for small ground heights, whereas the plates in dynamic ground effect have the positive pitching-moment coefficients for all ground heights.

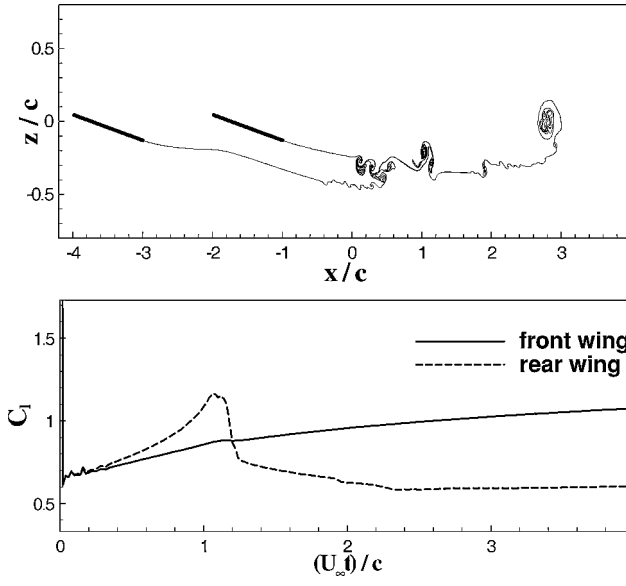

a) Out of ground effect

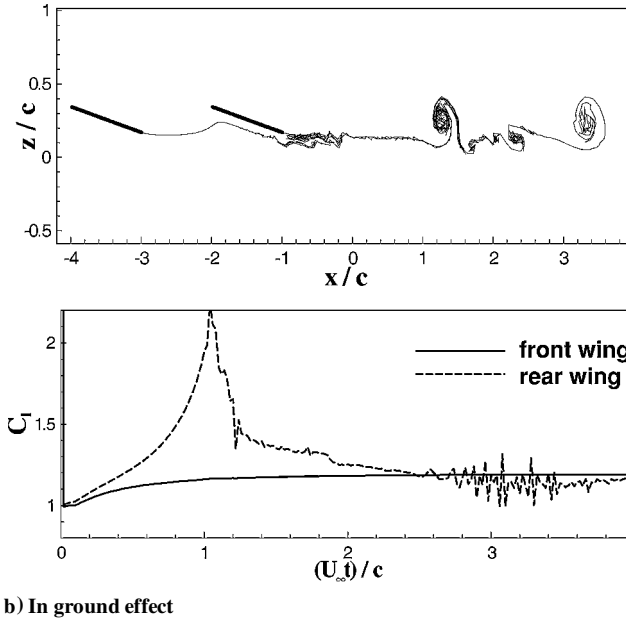

b) In ground effect

Fig. 7 Wake shapes and lift variations of tandem flat plates in sudden acceleration motion.

Figure 10 shows the aerodynamic coefficients of the plates in static ground effect. In the calculation the same angle of attack and flight-path angle as used in Fig. 9 are selected. In the figure the total lift coefficients of the plates are almost alike for three different distances between the plates. The pitching-moment coefficients become bigger as the distances decrease.

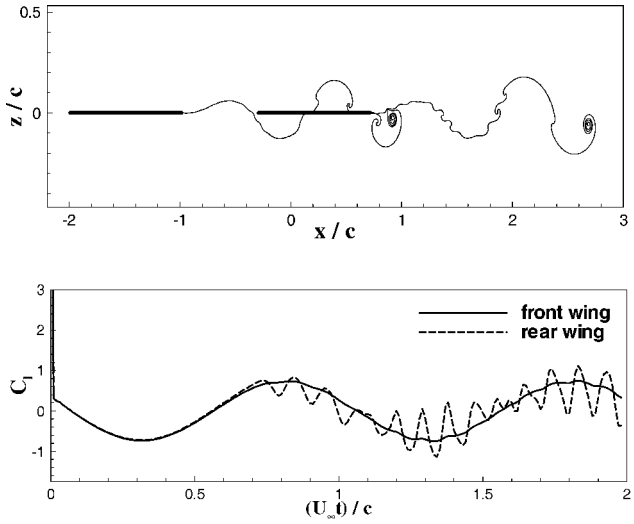

a) Out of ground effect

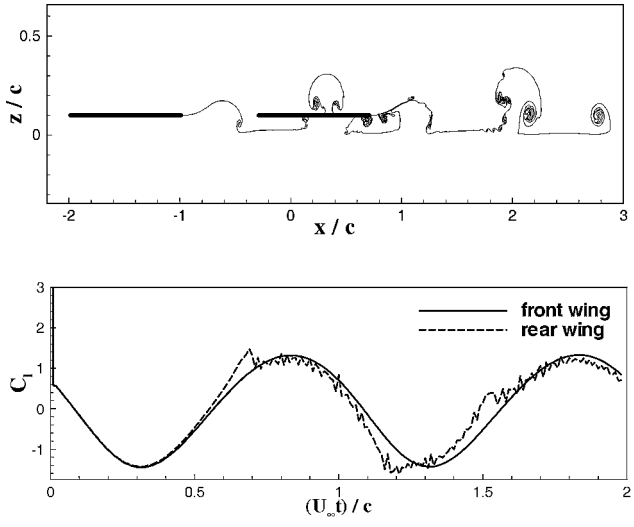

b) In ground effect

Fig. 8 Wake shapes and lift variations of tandem flat plates in heaving oscillation motion.

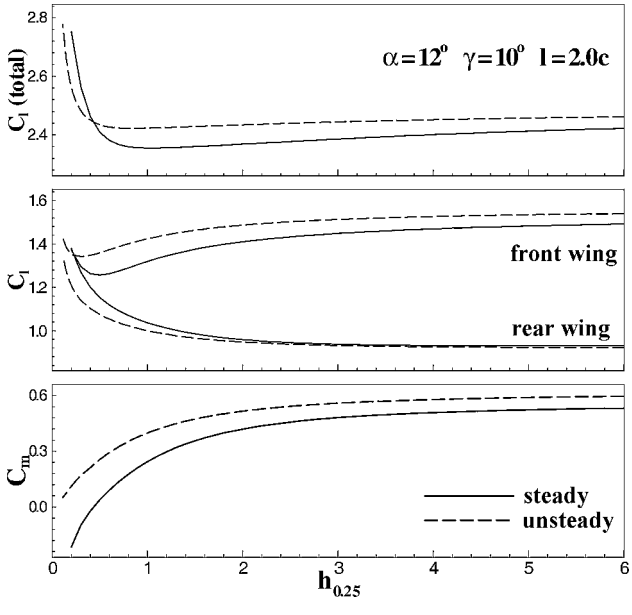

Fig. 9 Aerodynamic coefficients of tandem flat plates in static and dynamic ground effect.

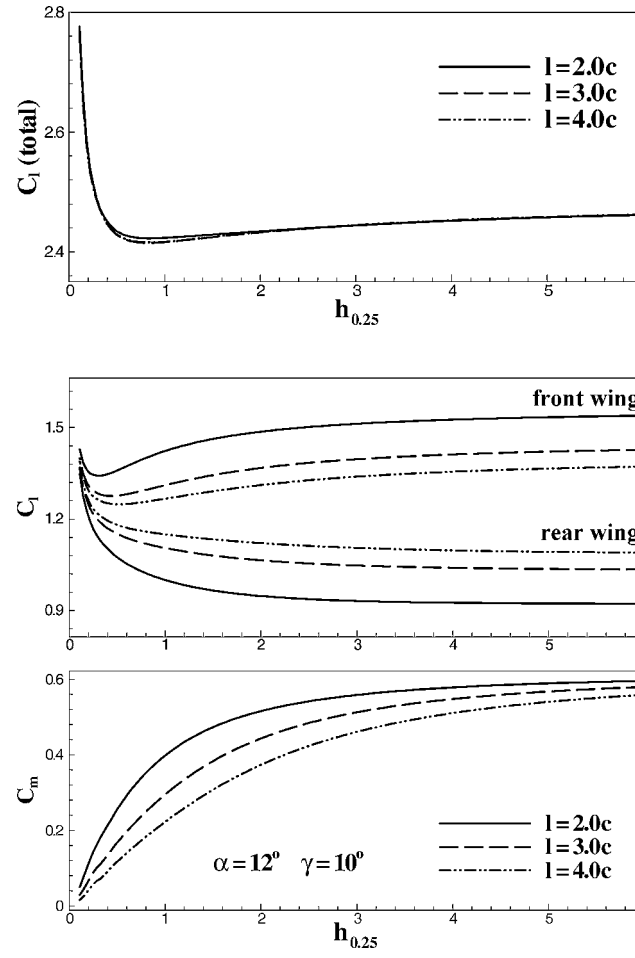

Fig. 10 Aerodynamic coefficients of tandem flat plates in ground effect for various distances between the plates.

IV. Conclusions

This study demonstrates that the use of a core addition scheme and the vortex core modeling reduces the computing time significantly while it produces the good representation of the wake pattern behind the flat plates in unsteady motion.

The prediction on the wake patterns shows that the unsteady ground effect complicates wake patterns more than the out-of-ground-effect case. This complicated wake pattern causes severe lift fluctuation on the plates. The investigated aerodynamic characteristics of tandem flat plates in dynamic ground effect are different from those of tandem flat plates in static ground effect. Although the present results are for the flat plates, it can be concluded that the dynamic ground effect can be of considerable importance in the prediction of the aerodynamic performances for the wings in tandem configuration.

Acknowledgment

This work was supported by Grant 1999-1-305-001-5 from the Basic Research Program of the Korean Science and Engineering Foundation.

References

[1]Kono, T., Kohama, Y., and Matsui, N., "Stability of Guide Way Type Wing in Ground Effect Vehicle," *Proceedings of the Third JSME-KSME Fluids Engineering Conference*, Sendai, Japan, 1994, pp. 715–718.

[2]Hiemcke, C., "NACA 5312 in Ground Effect: Wind Tunnel and Panel Code Studies," AIAA-97-2320, Reston, VA, 1997, pp. 829–838.

[3]Chen, Y. S., and Schweikhard, W. G., "Dynamic Ground Effects on a Two-Dimensional Flat Plate," *Journal of Aircraft*, Vol. 22, No. 7, 1985, pp. 638–640.

[4]Nuhait, A. O., and Zedan, M. F., "Numerical Simulation of Unsteady Flow Induced by a Flat Plate Moving Near Ground," *Journal of Aircraft*, Vol. 30, No. 5, 1993, pp. 611–617.

[5]Katz, J., "Calculation of the Aerodynamic Forces on Automotive Lifting Surfaces," *Journal of Fluids Engineering*, Vol. 107, 1985, pp. 438–443.

[6]Nuhait, A. O., and Mook, D. T., "Numerical Simulation of Wings in Steady and Unsteady Ground Effects," *Journal of Aircraft*, Vol. 26, No. 12, 1989, pp. 1081–1089.

[7]Rozhdestvensky, K. V., *Aerodynamics of a Lifting System in Extreme Ground Effect*, 1st ed., Springer-Verlag, Berlin, 2000, pp. 1–22.

[8]Sarpaka, T., "Computational Methods with Vortices—The 1988 Freeman Scholar Lecture," *Journal of Fluid Engineering*, Vol. 111, No. 1, 1989, pp. 5–52.

[9]Mook, D. T., Roy, S., Choksi, G., and Dong, B., "Numerical Simulation of the Unsteady Wake Behind an Airfoil," *Journal of Aircraft*, Vol. 26, No. 6, 1989, pp. 509–514.

[10]Ling, G. C., Bearman, P. W., and Graham, J. M. R., "A Further Simulation of Starting Flow Around a Flat Plate by a Discrete Vortex Model," *Internal Seminar on Engineering Applications of the Surface and Cloud Vorticity Methods*, Vol. 51, No. 14, 1986, pp. 118–138.

[11]Sarpkaya, T., and Schoaff, R. L., "Inviscid Model of Two-Dimensional Vortex Shedding by a Circular Cylinder," *AIAA Journal*, Vol. 17, No. 11, 1979, pp. 1193–1200.

[12]Polling, D. R., "Airfoil Response to Periodic Disturbances—The Unsteady Kutta Condition," Ph. D. Dissertation, Dept. of Engineering Mechanics, Virginia Polytechnic Inst. and State Univ., Blacksburg, VA, Aug. 1985.

[13]Ogawa, A., *Vortex Flow-CRC Series on Fine Particle Science and Technology*, CRC Press, Inc., Boca Raton, FL, 1993, pp. 203–213.

[14]Wieselsberger, C., "Wing Resistance Near the Ground," NACA TM-77, April 1922.

[15]Bratt, J. B., "Flow Patterns in the Wake of an Oscillation Airfoil," Aeronautical Research Council, R&M 2773, London, March 1953.